# Numerical investigation of concrete energy pile behavior in Winnipeg using coupled thermo-hydro-mechanical finite element analyses

Alitking Anongphouth, Pooneh Maghoul & Marolo Alfaro
*Department of Civil Engineering – University of Manitoba, Winnipeg, Manitoba, Canada*

ABSTRACT
Energy piles, used as ground heat exchanger elements in ground source heat pump systems to heat or cool building spaces, have been gaining popularity in recent years. It is important to understand the behavior of energy pile systems in local climatic and geotechnical conditions. This paper aims to investigate the behavior of the energy piles under climatic and geological conditions in Winnipeg, Manitoba. Coupled thermo-hydro-mechanical (THM) finite element analyses were carried out for hypothetical friction and end-bearing energy piles. These piles were subjected to both mechanical loads and six-year heating and cooling cycles. Numerical results are presented in terms of pile head displacements, strains, and loads developed in the piles, as well as skin friction, effective radial stresses along the pile-soil interfaces, and thermally induced excess porewater pressures in the surounding ground.

RÉSUMÉ
Les pieux géothermiques sont utilisés comme échangeurs thermiques dans les systèmes de pompes à chaleur géothermiques pour conditionner l'air des bâtiments; une pratique devenue populaire ces dernières années. Cet article vise à étudier le comportement des pieux géothermiques dans des conditions climatiques et géologiques de Winnipeg, Manitoba. Des analyses couplées thermo-hydro-mécaniques (THM) par la méthode des éléments finis ont été réalisées pour des pieux géothermiques hypothétiques flottants et chargés en pointe. Ces pieux ont été soumis à des chargements mécaniques et à des cycles de chauffage et de refroidissement pendant six ans. Les résultats numériques ont été présentés en termes de déplacements de la tête de pieu, de déformations et de charges développées dans les pieux, ainsi que de frottement latéral, de contraintes effectives radiales le long des interfaces pieu-sol et de pressions interstitielles excessives induites par le chargement thermique dans le sol.

## 1 INTRODUCTION

Shallow geothermal energy, which is the energy stored beneath the earth's surface in the form of heat, can be used for heating and cooling building spaces through ground source heat pump (GSHP) systems. In general, the shallow ground temperature within 50 m below the ground surface, in its natural state without any effects of human activities and other anomalies, usually ranges from 10 to 20°C (Al-Khoury, 2012). Similarly, Brandl (2006) reported values of 10 to 15°C and 20 to 25°C in Europe and the tropics, respectively. In Canada, as reported by Mitalas (1987), the mean annual ground temperature ranges from 4.6 to 12.3°C within 50 m below the ground surface. The value in Winnipeg (MB) is about 7°C and could even be higher in the urban center because of heat island effects (Ferguson & Woodbury, 2004).

Structural elements that are installed in the ground or in contact with the ground, collectively called energy geostructures, can be used as ground heat exchangers for the GSHP systems (Brandl, 2006). Among the energy geostructures, energy piles are the most widely used. In recent years, even though the use of energy piles has increased due to their energy effectiveness, renewability, and environmental friendliness, their acceptance and implementation has still been slow in some countries. This may be due to safety concerns of the developers/owners of buildings regarding possible adverse effects of heating-cooling cycles on the structural and geotechnical performances of the working piles, i.e., thermally loading the piles may lead to over-stressing of the concrete, loss of load-carrying capacities of the piles, and excessive settlements. Currently, there is still limited understanding of energy pile behavior under combined effects of thermal and mechanical loads, especially in cold regions like Canada. Comprehensive understanding of their structural and geotechnical performances is vital for successful applications. This paper aims to investigate responses of concrete energy piles subjected to thermal and thermo-mechanical loads using coupled thermo-hydro-mechanical (THM) finite element analyses. Two hypothetical energy piles in Winnipeg were analyzed to study their performances by considering local stratigraphical and climatic conditions. Results from these analyses could provide insights into the behavior of energy piles under these local conditions.

## 2 STRATIGRAPHY OF WINNIPEG

The top 3 m below the ground level (bgl), consisting of interbedded layers of the silty clay and silt with varying amounts of organic matter, is known locally in Winnipeg as the Upper Complex Zone (Baracos et al., 1983). This Upper Complex Zone is heavily fissured and has a nuggetty structure because of intense physical weathering. The thickness of the Winnipeg lacustrine clay underneath the Upper Complex Zone is typically about 9 to 12 m. Underlying the lacustrine clay is the till deposit with a typical thickness ranging from about 3 to 6 m but could be

as thick as 9 m in some locations. It usually contains 40 to 60 % of fines in the matrix with frequently predominant silt sizes. Because of this, the Winnipeg till is often locally known as the silt till. Underlying this silt till deposit is carbonate bedrock consisting primarily of dolomite and dolomitic limestone (Skaftfeld, 2014). The depth to the bedrock varies, generally ranging from about 15 to 21 m bgl.

## 3 NUMERICAL MODEL DESCRIPTION

Axisymmetric THM finite element analyses using PLAXIS 2D software were carried out for energy piles. Note that in this paper the negative sign (-) is used for compression and positive sign (+) is used for tension. Currently, there are no actual energy piles installed in Winnipeg. Generic energy friction and end-bearing piles were hypothesized based on local pile foundation engineering practice. The friction energy pile was assumed to have a diameter of 0.4 m and a length of 12 m installed entirely in the Winnipeg lacustrine clay. Similarly, the end-bearing energy pile was assumed to be 0.8 m in diameter and 20 m in length. The pile toe was assumed to be embedded 5 m into the very dense silt till.

### 3.1 Material Characteristics

For numerical modeling, the soil profile was generalized and consists of three main layers, disregarding the Upper Complex Zone. The first layer is the Winnipeg lacustrine clay, from 0 to 15 m bgl. This layer is underlain by the silt till, from 15 to 21 m bgl. Below the till is dolomitic limestone bedrock, extending to a great depth. The groundwater table at 3 m bgl was used in the models. The concrete pile was modeled as non-porous (solid) elastic material using linear elastic constitutive model (LEM). Hardening soil with small strain stiffness model (HSSM) was used for the clay and till. The LEM was also used for the dolomitic limestone. Table 1 shows some material parameters used for the numerical modeling of Winnipeg energy piles. Note that effects of temperature changes on mechanical properties of soils were ignored.

### 3.2 Model Geometry and Boundary Conditions

It was assumed that the energy piles were located underneath the center of the building with a 30 m width and without any basements. With these assumptions, an axisymmetric model was used. The model domain was set at a distance of 50 m (> 2L) and 75 m (> 3L) for the side and bottom boundaries, respectively, as illustrated in Figure 1. The model domain was divided into zones for the discretization in which very fine mesh sizes were used for the pile body, along the pile-soil interface, and around the pile toe. The mesh sizes were coarser for the zones further away from the pile. The 15-node triangular elements were used, providing a fourth order interpolation for displacements and numerical integrations involve 12 stress points. Interface elements with a strength reduction factor of 1.0 were assigned along the pile-soil interface.

Free displacements were allowed at the top of the model. Both vertical and radial displacements were restrained at the bottom boundary. Only vertical displacements were allowed at the left-hand side and right-hand side boundaries. The drainage was allowed at the top and right-hand side boundaries. A closed flow boundary was assigned along the axisymmetric line and the bottom of the model. The heat flow was closed at the right-hand side and left-hand side boundaries. At the top, the indoor air temperature (20°C) was used as a boundary condition inside the building while the outdoor air temperature was used outside the building. Figure 2 shows the observed seasonal variation of the mean daily air temperature at the Winnipeg Richardson International Airport (ECCC, 2016).

A constant ground temperature of 7°C was assigned at the bottom boundary. The initial ground temperature for the entire model domain was also set at 7°C which is approximately the undisturbed average ground temperature in the Winnipeg area (Ferguson and Woodbury, 2004; Mitalas, 1987). The concrete slab-on-grade was not placed in the models. However, its effect was represented using the convective thermal boundary with the assumed overall thermal transmittance value (U-value) of $0.2\text{x}10^{-3}$ kW/m$^2$/ºC. This value was assumed based on Thomas and Rees (1999) which reported the measured U-values of 0.26 and $0.20\text{x}10^{-3}$ kW/m$^2$/C for the insulated concrete slab-on-grade using the normal weight

Table 1. Some material parameters used for numerical modeling of the Winnipeg energy piles

| Parameter | Winnipeg clay | Silt tilt | Dolomitic limestone | Concrete pile |
|---|---|---|---|---|
| Elastic modulus, E' (kPa) | - | - | $11000\text{x}10^3$ | $40000\text{x}10^3$ |
| Poisson's ratio (Un/reloading Poisson's ratio), $\nu$' ($\nu_{ur}$) | (0.2) | (0.2) | 0.2 | 0.15 |
| Reference secant stiffness, $E^{ref}_{50}$ (kPa) | $21\text{x}10^3$ | 110x103 | - | - |
| Reference tangent stiffness, $E^{ref}_{oed}$ (kPa) | $21\text{x}10^3$ | 110x103 | - | - |
| Reference un/reloading stiffness, $E^{ref}_{ur}$ (kPa) | $63\text{x}10^3$ | 330x103 | - | - |
| Exponential power, m (-) | 1 | 0.5 | - | - |
| Reference shear stiffness at very small strain, $G^{ref}_o$ (kPa) | $84\text{x}10^3$ | 440x103 | - | - |
| Threshold shear strain, $\gamma_{0.7}$ (-) | 0.0002 | 0.0002 | - | - |
| Effective cohesion, c' (kPa) | 3 | 3 | - | - |
| Effective internal friction angle, $\phi$' (°) | 23 | 40 | - | - |
| Hydraulic conductivity, $k_x$, $k_y$ (m/day) | $6.70\text{x}10^{-5}$ | 0.028 | 8.64 | - |
| Specific heat capacity, $c_s$ (kJ/t/°C) | 830 | 720 | 1300 | 800 |
| Thermal conductivity, $\lambda_s$ (kW/m/°C) | $1.2\text{x}10^{-3}$ | $1.5\text{x}10^{-3}$ | $2.3\text{x}10^{-3}$ | $1.8\text{x}10^{-3}$ |
| Linear thermal expansion coefficient, $\alpha_{sL}$ (1/°C) | $5\text{x}10^{-6}$ | $5\text{x}10^{-6}$ | $5\text{x}10^{-6}$ | $10\text{x}10^{-6}$ |

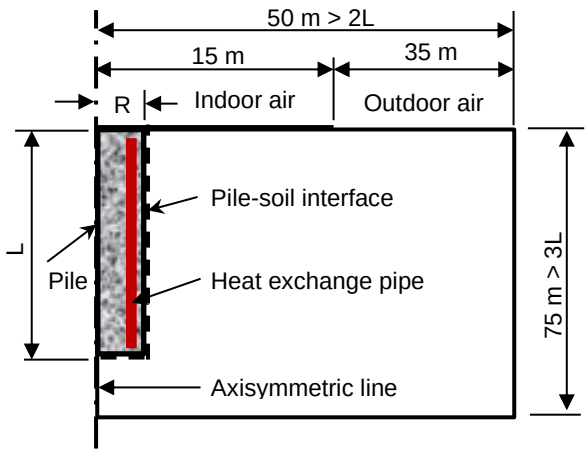


Figure 1. Axisymmetric geometry setup for Winnipeg energy piles (not to scale)

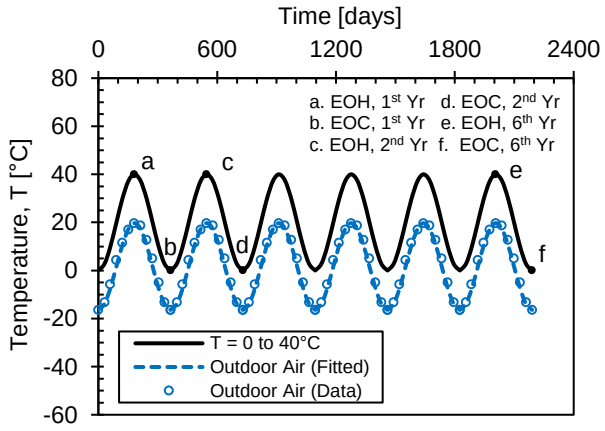


Figure 2. Outdoor air temperature variation and thermal loads applied to the pile in terms of temperature variation starting from the 1st of January

concrete and light weight concrete, accordingly. The convective boundary condition was also applied along the ground surface outside the building with the assumed overall U-value of $15x10^{-3}$ kW/m$^2$/ºC. This value was used because it provided the simulated frost depth of about 2.0 m bgl, which is close to the frost depth of 1.8 m bgl reported in Winnipeg (Baracos et al., 1983). However, the frost depth may vary from place to place, depending on the local conditions such as the ground surface cover materials and vegetation.

A mechanical load was applied on the pile head in a drained manner before the heating-cooling cycles began. The mechanical loads were assumed to be equal to working loads of the piles, estimated using the semi-empirical static method and based on typical geotechnical properties of Winnipeg's soils. The estimated working load of the friction pile was -235 kN (compression), corresponding to the stress on the pile head of -1870 kPa. Similarly, for the end-bearing pile, these values were -1300 kN and -2586 kPa.

In addition to the structural loads, the energy piles are also subjected to thermal cycles. In this study, a temperature range (T) as a function of time from 0 to 40°C was used, as shown together with the outdoor air temperature variation in Figure 2. The convective boundary condition at 70 mm from the pile shaft was used to represent the heat exchange pipe. It was assumed that the changing pattern of the temperature in the pile with time generally followed the rising and falling pattern of the seasonal outdoor air temperature. The assumption was made based on the field observation by Brandl (2006) on the operational energy geostructures. The energy piles were subjected to six heating-cooling cycles, corresponding to six years of heating and cooling of the building. Here, the term at the end of heating (EOH) means the pile was heated to the maximum temperature (the peak). Likewise, the term at the end of cooling (EOC) means the pile was cooled to the minimum temperature (the trough) in the particular year.

## 4 RESULTS AND DISCUSSIONS

### 4.1 Temperature Distributions

Temperature profiles along the pile-soil interface at the end of heating (EOH) and end of cooling (EOC) for the friction energy pile are provided in Figure 3. The temperatures were relatively constant with depths, except reductions (roll-offs) near the pile head and pile toe due to mechanisms of heat transfer at this pile ends. The temperatures slightly increased with increasing simulation times. At mid depth of the pile, the temperature was 37.14ºC at the EOH in the 1st year, comparing with 37.64ºC in the 6th year (an increase of 1.34%). Even though this difference is insignificant, it shows that temperatures along the pile-soil interface trend to increase with time. This may be due to the influence of heat loss through the ground floor slab that accumulated in the ground underneath the building with time. At the EOC, the temperature profile in the 6th year was somewhat higher than in the 1st year. In the radial direction, at the EOH, the temperatures dropped sharply from the pile center to 2 m away. Outside this distance, the changes in temperatures were small. Likewise, at the EOC, the temperatures increased steeply from the center of the pile to a distance of about 2 m. There were minimal changes beyond this point. Similar observations were found for the end-bearing pile, temperatures along the pile-soil interface were relatively constant in the clay layer. Small reductions in the till layer were detected that may be due to lower specific heat capacity and higher thermal conductivity of the till. The roll-offs of temperature values were again observed near the pile ends. There were little changes (only increased from 38.53 to 38.73ºC and from 7.94 to 8.91ºC) in the maximum temperature values at the EOH and EOC from the first to sixth year, respectively. Nonetheless, the ground temperature seems to increase with time.

### 4.2 Excess Porewater Pressure Distributions

Excess porewater pressures (EPWPs) were induced in the clay due to its low hydraulic conductivity. Heating produced negative EPWPs with the maxumum values of -6.74, -6.36,

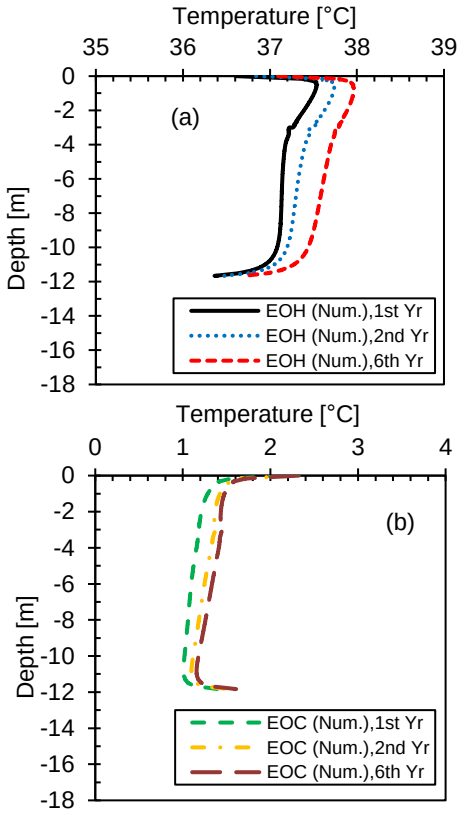


Figure 3. Temperature profiles along the pile-soil interface (a) at the end of heating (EOH) and (b) at the end of cooling (EOC) in the 1st, 2nd, and 6th year for the friction energy pile

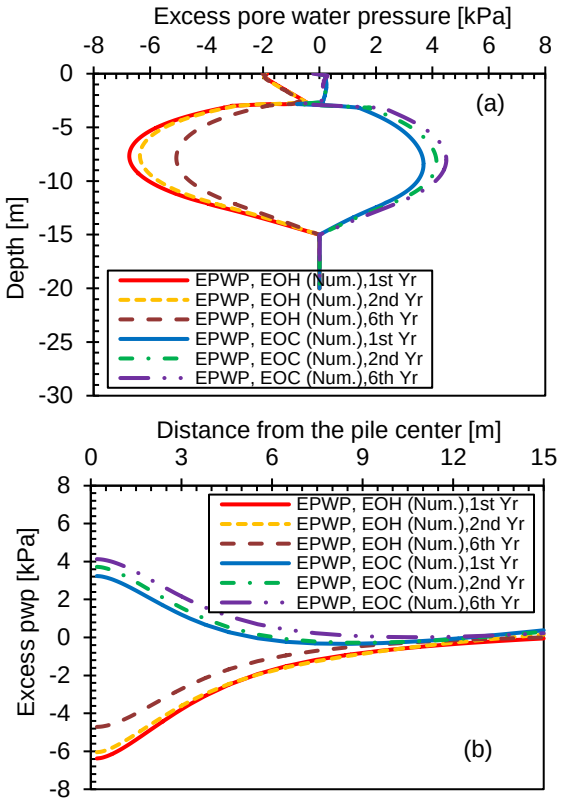


Figure 4. Thermally induced excess porewater pressures (a) along the pile-soil interface to 20D below the pile toe and (b) at mid-depth of the pile from the pile center to 15 m away in the 1st, 2nd, and 6th year for the friction energy pile

and -5.07 kPa at the EOH in the 1st, 2nd, and 6th year, accordingly, as illustrated in Figure 4(a). In a similar situation from energy pile centrifuge tests in clay, Ng et al. (2014) found that the EPWPs reduced from -34 kPa in the first thermal cycle to -24 kPa in the fifth cycle. As the numerical results shown, the EPWPs at the EOH in the Winnipeg clay adjacent to the energy pile also slightly reduced with time (about 6% reduction from the 1st to 6th year. This reduction in EPWPs may be partially due to the dissipation of EPWPs with time (consolidation). Another reason may have resulted from the lesser temperature difference between the pile and surrounding ground at the end of heating due to overall ground warming. This overall ground warming was caused by heat loss from the ground floor slab, accumulating through time and also the imbalance in thermal loads during heating and cooling periods in relation to the initial ground temperature. The opposite occurred during cooling in which the possitive EPWPs were generated with the maximum values of 3.69, 4.15, and 4.49 kPa at the EOC in the 1st, 2nd, and 6th year, respectively. Therefore, the positive EPWPs increased with time by 3.5% from the 1st to 6th year, resulting from the larger temperature difference between the pile and surrounding ground at the EOC due to overall ground warming. Figure 4(b) shows the EPWP profiles through a horizontal cross-section at mid-depth of the pile from the pile-soil interface to 15 m away. The change in EPWPs occurred within a distance of 8 m (20D) from the pile-soil interface with maximum values adjacent to the pile. These EPWP responses also happened in the clay layer from the end-bearing energy pile analyses, even though not shown here.

### 4.3 Pile Head Vertical Displacements

Simulated vertical pile head displacements during six-year heating and cooling cycles are shown in Figure 5(a), for the friction pile. The mechanical load (M) caused a pile head settlement of -2.0 mm (-0.50%D). When the pile heated, uplifts were induced. In contrast, when the pile was cooled, settlements occurred. The uplift-settlement trend moved downwards gradually when the number of thermal cycles increased. These ratcheting settlements were probably due to the accumulated plastic strains occurred in the surrounding soils which; in turn, caused by thermal cyclic loading. As also mentioned in GSHPA (2012) that applying thermal cycles repeatedly on the energy pile would result in accumulated settlements. The settlements may be also partially due to the consolidation of the clay with time. The pile head uplifts due to thermo-mechanical loads at the EOH in the 1st and 6th year were 0.28 mm (0.07%D) and 0.04 mm (0.01%D), correspondingly. This gave a reduction in the pile head uplift of 85.71%. At the EOC in the 1st and

6th year, the pile head settlements were -0.85 mm (0.21%D) and -0.96 mm (0.24%D), leading to an increase in the settlement of 13%. As for the end-bearing energy pile, Figure 5(b) shows the simulated vertical pile head displacements for six-year heating and cooling cycles. The mechanical load (M) caused a pile head settlement of -1.89 mm (-0.24%D). Again, the thermal cycles caused ratcheting settlements of the pile head. At the EOH in the 1st and 6th year, the uplifts of the pile head of 2.78 mm (0.35%D) and 0.52 mm (0.07%D) were obtained, a drop of 81%. On the other hand, the settlements at the EOC in the 1st and 6th year were -4.18 mm (-0.52%D) and -5.91 mm (-0.74%D), increasing by 41%. These ratcheting settlements were also noticed in the centrifuge tests of energy piles in clay subjected to five thermal cycles (Ng et al., 2014).

### 4.4 Pile Axial Strains

For the friction energy pile, the mechanical load (M) produced contractive strains (negative) in the entire pile length as shown in Figure 6(a). The expansive strains (positive) were induced due to the thermal heating in contradiction with the mechanical load as shown in Figure 6(b). The thermo-mechanically induced strains are illustrated in Figure 6(c). At the EOH, slightly lower strains were observed with shorter simulated times, 1st, 2nd, and 6th year, accordingly. Cooling the pile generated contractive strains, as shown in Figure 7, with lower contractive strains at the EOC in the 6th year. Although not shown here, these axial strain development phenomena also observed for the end-bearing energy pile.

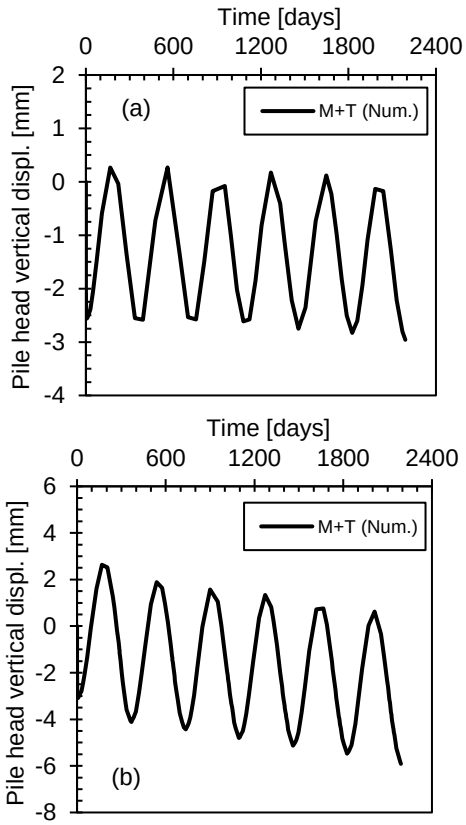


Figure 5. Pile head vertical displacements during six-year cooling and heating cycles (a) friction energy pile and (b) end-bearing energy pile

### 4.5 Pile Axial Loads

Axial load profiles generated in the friction energy pile are given in Figure 8. The mechanical load profile was plotted in all figures for a reference. It can be seen that the mechanical load of -235 kN applied on the pile head transferred to the surrounding ground, reducing with the depth almost linearly. As shown in Figure 8(a), thermally induced compressive loads due to heating in the pile were lower with longer simulated times. This was due to the smaller temperature difference in the pile and the surrounding ground caused by the overall warming of the

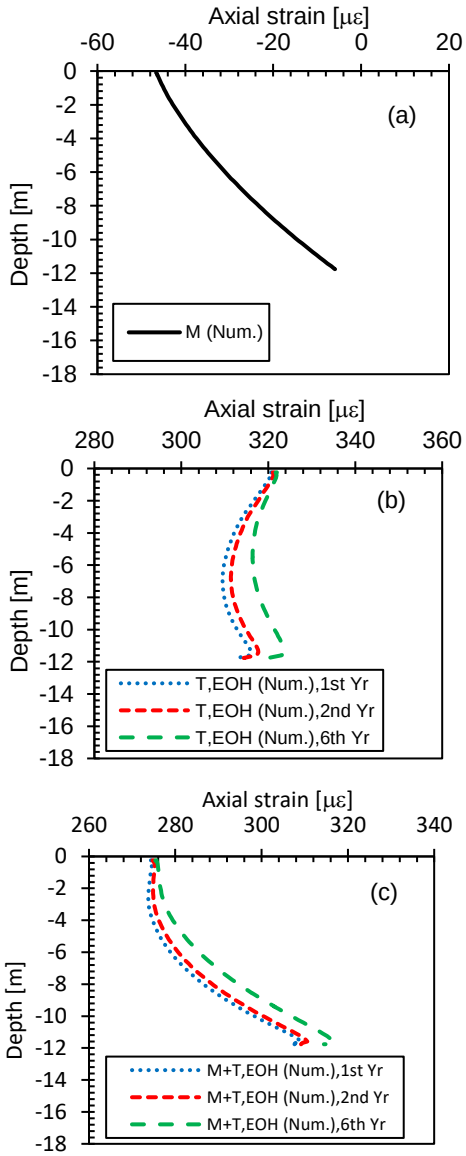


Figure 6. Axial strain profiles due to (a) mechanical load (M), (b) thermal (T), and (c) thermo-mechanical (M+T) at the end of heating (EOH) in the 1st, 2nd, and 6th year for the friction energy pile

model domain. The maximum values at the EOH in the 1st, 2nd, and 6th year were -109.09, -96.23, and -70.74 kN, accordingly. This gave a fall of 35% from the 1st to 6th year. The thermo-mechanically induced compressive load profiles at the EOH are shown in Figure 8(b) with the highest in the 1st year (-293.26 kN). The load values then reduced with simulated times, reaching -277.57 kN in the 6th year (a fall of 5%). In contrast to the heating, the cooling induced tensile loads (positive) in the pile. Therefore, the thermo-mechanically induced loads at the EOC reduced along the pile length, especially in the lower part near the pile toe. In the 6th year, slightly higher thermally induced tensile loads were produced (78.69 kN max.) in comparison with the values in the 1st year (66.48 kN max.) and 2nd year (68.71 kN max.). i.e., an increase of 15.52% from the 1st to the 6th year. The combined effects of thermal and mechanical loads (M+T, EOC) also created small tensile loads near the pile toe.

As for the end-bearing energy pile, the maximum mechanical load was at the pile head (-1300 kN). This mechanical load transferred mostly into the much stronger till layer, located below -15 m. Note that the axial load profiles at the EOH are not shown here. The thermally induced compressive loads were -699.26 kN at the EOH in the 1st year. This value reduced to -654.31 kN in the 6th year (a fall of 6.43%). The axial compressive loads increased in the pile as a result of thermo-mechanical loads. This was because heating induced additional compressive loads in the pile. The maximum value of -699.26 kN occurred in the 1st year. The values reduced marginally for the later years, reaching -651.31 kN in the 6th year (6.86% decrease). Considerable tensile loads were generated in the pile during cooling, as shown in Figure 9. At the EOC, the maximum values were 493.72 kN (1st year), 554.94 kN (2nd year), and 648.46 kN (6th year). This shows an increase in thermally induced tensile load of 31.34% from the 1st to 6th year. Even though there were large reductions of the mechanical loads due to pile cooling, no tensile loads were induced for the thermo-mechanical effects.

### 4.6 Mobilized Skin Friction

Mobilized skin friction along the pile-soil interface at the EOH and at the EOC in the 1st, 2nd, and 6th year are illustrated in Figure 10. The positive skin friction was mobilized along the entire pile length due to the mechanical load (M). During heating, the upper half of the pile, above the neutral plane (NP) - a reference point where the pile did not displace, moved upwards relative to the surrounding soils, causing the skin friction to decrease. This led to negative skin friction (acting downwards). In the lower half, on the other hand, the pile moved downwards and induced higher skin friction. The opposite responses occurred during cooling in which the skin friction increased along the upper part. In the lower part near the pile toe; however, it reduced. This was because the pile contracted more in relation to the surrounding soils as the pile was cooled. As

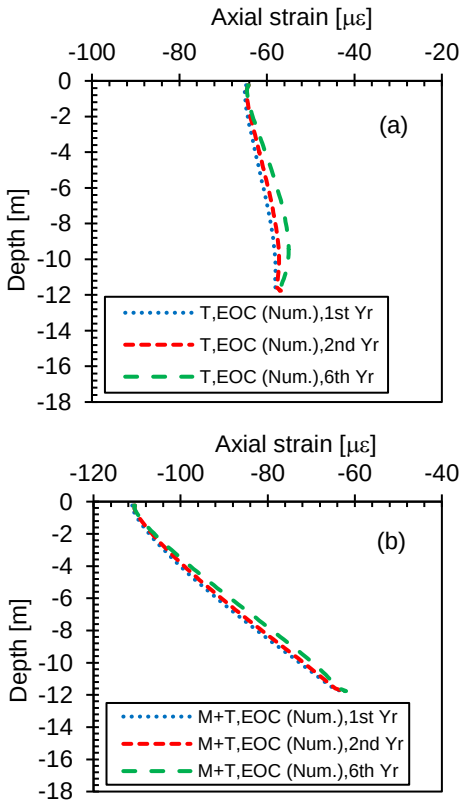


Figure 7. Axial strain profiles (a) thermal (T) and (b) thermo-mechanical (M+T) at the end of cooling (EOC) in the 1st, 2nd, and 6th year for the friction energy pile

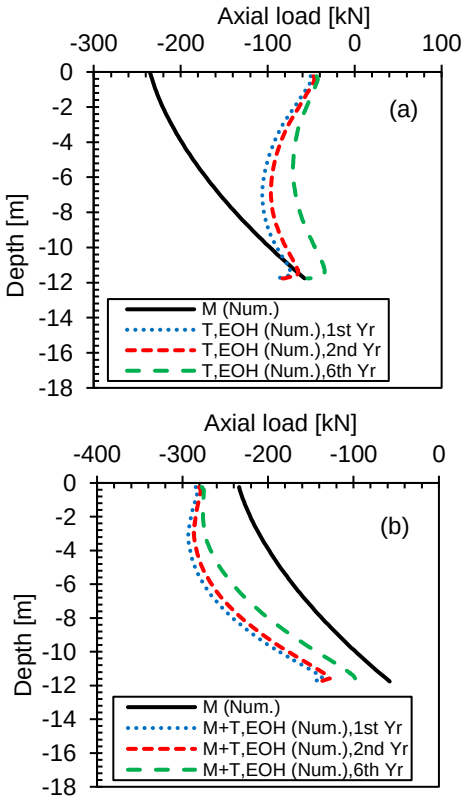


Figure 8. Axial load profiles (a) thermal (T) and (b) thermo-mechanical (M+T) at the end of heating (EOH) in the 1st, 2nd, and 6th year for the friction energy pile

seen in these figures, minimal changes in the skin friction profiles with different simulated times were also observed. Similar occurrences were noticed for the end-bearing energy pile during heating and cooling cycles. The skin friction profiles at the EOC are illustrated in Figure 11.

### 4.7 Mobilized Effective Radial Stresses

As seen in Figure 12(a), the effective radial stresses along the entire pile-soil interface increased due to heating. At the EOC, these stresses reduced in the lower part of the pile but marginally increased in the upper part near the pile head as shown in Figure 12(b). The same trends were also detected for the end-bearing energy pile as shown in Figure 13. The reasons for these phenomena may be due to the stress redistributions to somewhat compensate the reduction in stresses at the lower part of the pile and at the pile toe at the EOC. The change in effective radial stresses could be caused by a change in a lateral earth pressure coefficient (K) due to relative thermal expansions or contractions of the pile and the surrounding soils. The K values generally increased upon heating the pile-soil system and reduced upon cooling as reported in Gunawan et al. (2017). This makes sense because when the pile was heated it expanded and laterally pressed against the surrounding soils, producing higher K values and therefore higher effective radial stresses. Note that, there were slight differences among the results obtained from the different simulation times.

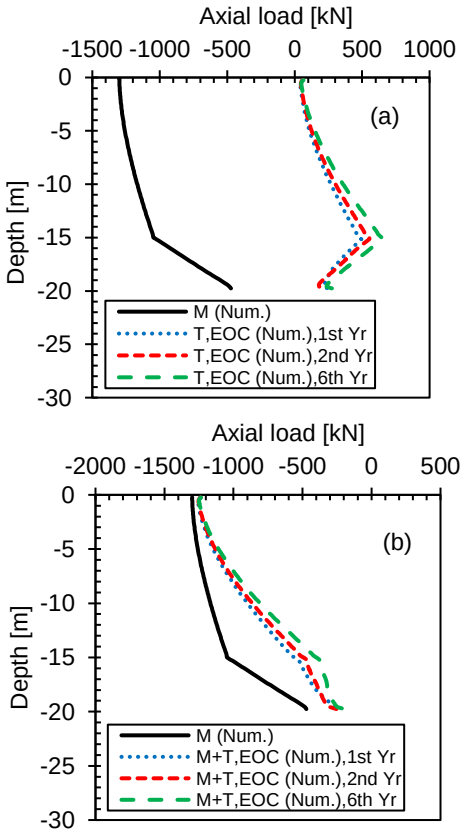


Figure 9. Axial load profiles (a) thermal (T) and (b) thermo-mechanical (M+T) at the end of cooling (EOC) in the 1st, 2nd, and 6th year for the end-bearing energy pile

## 5 CONCLUSIONS

In general, heating resulted in expansive strains in the piles. Thermally induced compressive loads were then

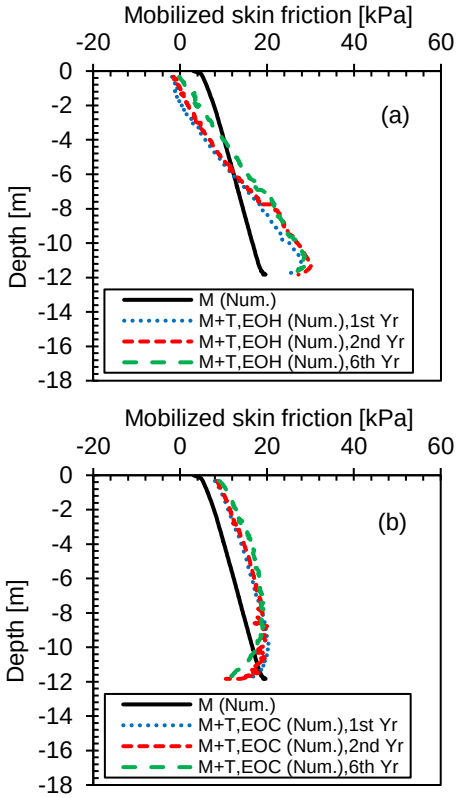


Figure 10. Mobilized skin friction along the pile-soil interface (a) at the end of heating (EOH) and (b) at the end of cooling (EOC) in the 1st, 2nd, and 6th year for the friction energy pile

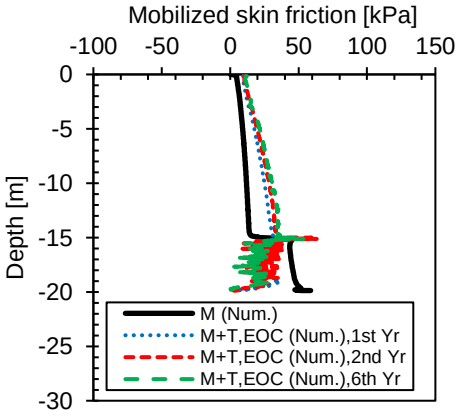


Figure 11. Mobilized skin friction along the pile-soil interface at the end of cooling (EOC) in the 1st, 2nd, and 6th year for the end-bearing energy pile

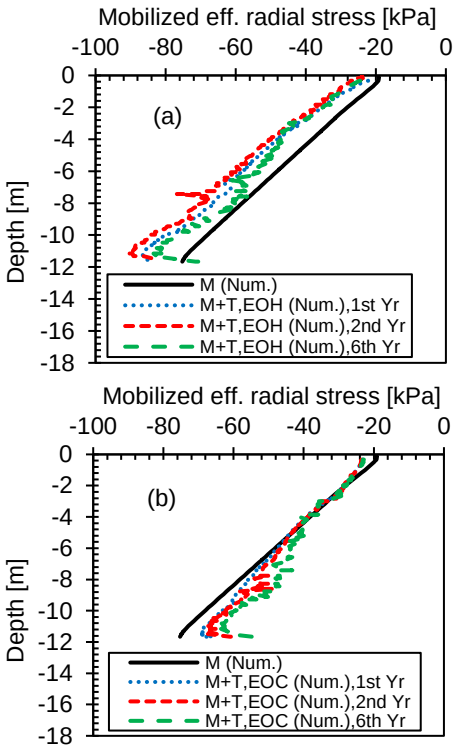


Figure 12. Mobilized effective radial stresses along the pile-soil interface (a) at the end of heating (EOH) and (b) at the end of cooling (EOC) in the 1st, 2nd, and 6th year for the friction energy pile

generated in addition to the mechanical loads. Therefore, for the thermal and mechanical combined effects, the compressive loads were higher during heating which may cause over-stressing of the piles if not appropriately considered in the design. Both friction and end-bearing energy piles showed a decreasing trend of thermally induced loads with time. Compressive strains were generated during cooling and led to tensile loads in the piles. For the thermo-mechanical combined effects, the compressive loads reduced and the tensile loads usually occurred near the pile toes, where the mechanical loads were small. These tensile loads may lead to tension cracks in the piles if not properly taken into account. The maximum thermally induced tensile loads at the EOC marginally increased with time. In terms of pile head displacements, heating produced uplifts of the pile heads while cooling caused settlements. Ratcheting settlement phenomena were observed for both energy piles. These may lead to long-term serviceability problems of the piles which should be considered in the energy pile design as well. The heating-cooling cycles also affected the surrounding ground temperatures to some distances. Excess porewater pressures (EPWPs) were generated in the Winnipeg clay layer due to its low permeability. The highest EPWPs were induced adjacent to the piles. The mobilized skin friction and the effective radial stresses along the pile-soil interfaces were also affected by the temperature changes to some extent.

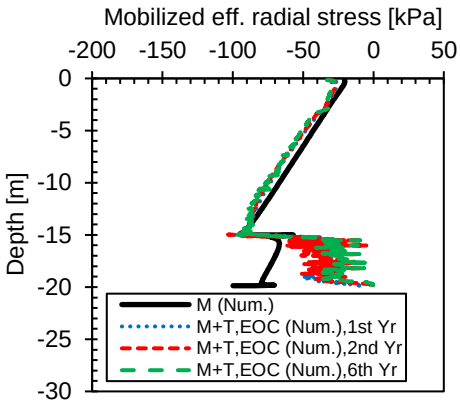


Figure 13. Mobilized effective radial stresses along the pile-soil interface at the end of cooling (EOC) in the 1st, 2nd, and 6th year for the end-bearing energy pile

REFERENCES


Al-Khoury, R. 2012. Computational Modeling of Shallow Geothermal Systems. CRC Press, Boca Raton. FL.

Baracos, A., Shields, D.H., and Kjartanson, B. 1983. Geological Engineering Report for Urban Development of Winnipeg. University of Manitoba.

Brandl, H. 2006. Energy Foundations and Other Thermo-Active Ground Structures. Géotechnique, **56**(2): 81–122.

ECCC. 2016. The Environment and Climate Change Canada (ECCC), Canadian Climate Normals 1981-2010 Station Data.

Ferguson, G., and Woodbury, A.D. 2004. Subsurface Heat Flow in an Urban Environment. Journal of Geophysical Research: Solid Earth, **109**(B2): 1–9.

GSHPA. (2012). *Thermal Pile Design, Installation and Materials Standards*. Ground Source Heat Pump Association, National Energy Centre.

Gunawan, A., Ng, C.W.W., and Liu, H. 2017. Effects of Cooling on the Ultimate Capacity of Energy Pile. *In* The 19th International Conference on Soil Mechanics and Geotechnical Engineering. pp. 3439–3442.

Mitalas, G.P. 1987. Calculation of Below-Grade Residential Heat Loss - Low-Rise Residential Building. ASHRAE Transactions, **93**: 743–783.

Ng, C.W.W., Shi, C., Gunawan, A., and Laloui, L. 2014. Centrifuge modelling of energy piles subjected to heating and cooling cycles in clay. Geotechnique Letters, **4**: 310–316.

Skaftfeld, K. 2014. Experience as a Guide to Geotechnical Practice In Winnipeg. M.Sc.Thesis, University of Manitoba.

Thomas, H.R., and Rees, S.W. 1999. The Thermal Performance of Ground Floor Slabs - A full Scale In-Situ Experiment. Building and Environment, **34**: 139–164.